Chemiresistors for the Real#Time Wireless Detection of Anions

: 10.1002/((please add manuscript number))
Article type: Full Paper

Chemiresistors for the Real-Time Wireless Detection of Anions

*By Seon-Jin Choi, Bora Yoon, Jason D. Ray, Anton Netchaev, Lee C. Moores, and Timothy M. Swager**

Prof. T.M. Swager, Dr. S-J Choi
Department of Chemistry,
Massachusetts Institute of Technology,
Cambridge, Massachusetts 02139, United States
*E-mail: tswager@mit.edu

Dr. B. Yoon
Optical and Electromagnetic Materials Team,
U.S. Army Combat Capabilities Development Command–Soldier Center (CCDC–SC),
Natick, Massachusetts 01760, United States

Prof. T.M. Swager, Dr. B. Yoon
Institute for Soldier Nanotechnologies,
Massachusetts Institute of Technology,
Cambridge, Massachusetts 02139, United States

Mr. J.D. Ray, Dr. A. Netchaev
U.S. Army Engineer Research and Development Center,
Information Technology Laboratory,
3909 Halls Ferry Road, Vicksburg, Mississippi 39180

Dr. L.C. Moores
U.S. Army Engineer Research and Development Center,
Environmental Laboratory,
3909 Halls Ferry Road, Vicksburg, Mississippi 39180

Keywords: Single-walled carbon nanotubes; squaramide; anion sensing; hydrogen bonding; deprotonation

Abstract

We report an electrical transduction platform for real-time wireless anion sensing using single-walled carbon nanotubes (SWCNTs) noncovalently functionalized with squaramide-based anion binding selectors. We systematically studied an anion binding properties and efficiency of the electrical transduction of the functionalized SWCNT composites using the squaramide-based selectors with two similar electron withdrawing groups, 3,5-bis(trifluoromethyl)benzyl (**1**) and 3,5-bis(trifluoromethyl)phenyl (**2**), which induce hydrogen bonding interaction with anions and deprotonation of a squaramide N–H proton upon addition of acetate (AcO^-), respectively. Charge transduction occurs with AcO^- as a result of charge transfer from the deprotonated selector **2**, whereas less sensitive transduction was observed with selector **1** via hydrogen bonding interaction. These results provide guidelines to efficiently transduce the chemical interaction between selectors and anions to create resistive transduction with functionalized SWCNTs. Electron withdrawing groups adjacent to the squaramide as well as proximate cationic pyridyl groups, enhance the anion binding affinity and also lower the selector's pK_a. The chemiresistive sensor arrays are readily integrated with a wireless sensing module and demonstrated real-time sensing of multiple anions with a smartphone readout.

1. Introduction

Anion recognition and sensing are of increasing importance in healthcare, biology, environment, and military applications.[1-3] In particular, real-time analysis of a trace amount of specific anions is crucial to the monitoring of the physical and metabolic states of biological systems. For example, minimizing acetate accumulation during rapid growth of bacteria cells is one of the major challenges in industrial biotechnology for maximized production of recombinant proteins, wherein acetate is a physiological switch that controls the growth rate of bacterial cells.[4, 5] In addition, monitoring chloride concentrations in sweat is an important biomarker for diagnosis of cystic fibrosis.[6] Ongoing and previous advances in anion supramolecular chemistry enable the ability to create specificity via receptors and selectors for the detection of key species.

Various coordination techniques have been employed for the recognition of anions. Among these, hydrogen-bonding anion receptors represent the most widely investigated and efficient binding strategy. In particular, dual-hydrogen bonding donors such as squaramides form stable six- and eight-membered chelate rings upon anion complexation of halide and oxoanion ions, respectively.[7] In addition, theoretical and experimental studies demonstrated that squaramide possesses stronger binding affinity compared to urea analogues as a result of the increased aromatic character of the squaramide ring with anion complexation.[8] The acidities of squaramides have recently been investigated as a fundamental physical organic parameter and point to their more acidic nature, relative to ureas, as important to their anion recognition properties.[9, 10] Building upon this understanding, a number of squaramide derivatives have been designed and investigated for colorimetric anion sensing,[11] transmembrane anion transporters,[12] optical imaging in cells,[13, 14] and organocatalysts.[15, 16]

Complementary electrostatic interactions can enhance anion binding affinity even in aqueous media. Recent examples include the use of cationic guanidinium,[17] imidazolium,[18-20] and pyridinium groups.[21, 22] Indeed, a comparative investigation of electrostatic

interactions in anion binding affinity revealed an increase in benzoate binding with a N-methyl pyridinium (K_a=300 M^{-1}) as compared to the analogous pyridine-amide receptor (K_a=16 M^{-1}) in DMSO-d_6.[23]

NMR and UV-vis methods are useful for the study of anion supramolecular chemistry as well as elucidating the receptor-anion structures and binding affinity.[24, 25] Nevertheess, portable and real-time anion detection techniques will enable high-throughput screening for industrial applications wherein rapid analysis with minimal amounts of sample necessary. Electrochemical analysis exploiting redox properties of selectors have been widely investigated for the rapid and potentially portable anion sensing of halide anions.[26-28] However, compatible integration of sensor arrays with wireless sensing module and minimal consumption of analyte samples for sensing are still challenging. To this end, development of anion microsensors that can produce simple output signals are needed.

Chemical sensors using carbon nanotubes (CNTs) transduction have been intensively studied by investigating transitions wherein the carrier transport is modulated by chemical interactions on the graphene sidewalls.[29, 30] Selectivity and high sensitivity are achieved by functionalization with selectors that promote chemical interactions with selected analytes.[31, 32] Nevertheless, chemiresistive anion sensing using carbon nanotubes remains a challenging as a result of mechanical instabilities of the sensor materials and non-specific charge transfer in complex aqueous solutions.

In our previous studies, mechanically a robust sensing platform was successfully developed by noncovalently wrapping of single-walled carbon nanotubes (SWCNTs) with poly(4-vinylpyridine) (P4VP) and then covalently anchoring this complex to a glass substrate.[33-36] The pyridyl groups from P4VP afford additional post-functionalization of the immobilized SWCNT assemblies with analyte specific selectors. For example, enzyme functionalization of alkylated P4VP/SWCNT was used to create robust sensors for glucose

analysis .[36] For the present study, that quaternization of pyridyls to produce pyridinium groups enhances anion binding affinity by electrostatic interactions.

We report herein an efficient and portable sensing platform for the transduction of anion binding events to create electrical signals, which makes use of squaramide-based selectors enhanced by proximality to a cationic pyridinium moieties that wrap the SWCNTs. This platform has capability for real-time detection of multiple anions in small samples (2 μL) by wireless communication methods.

2. Result and Discussion

We describe herein an anion sensing platform for efficient transduction by electrical resistance changes using two selectors (**Figure 1a**). The electrical transduction elements are formed from SWCNTs wrapped with P4VP that are chemically immobilized on a glass substrate by reaction of pyridyl groups from P4VP with alkyl bromides on a glass substrate (Figure 1b). Dual-hydrogen bonding donor, squaramide-selectors were covalently linked the P4VP-SWCNT with the goal of creating sensitivity to target anions. We have investigated squaramide-based selectors having 3,5-bis(trifluoromethyl)benzyl (**1**) and 3,5-bis(trifluoromethyl)phenyl (**2**) groups to compare anion binding affinities and their electrical transduction. As part of the selector functionalization, cationic pyridinium are produced that synergistically interact with anions to enhance binding.

We began by investigating changes in free energy (ΔG) before and after complexes with anions using density functional theory (DFT) calculations. Model squaramide-based selectors were generated that contain the cationic moiety (pyridinium) and the electron withdrawing groups of **1** and **2** (Figure S1). ~~The bromine counterion of model selectors has its origin from the alkyl bromide that reacts with the pyridyl group. The selector's counterion will exchange with anions having stronger binding affinities. The effect of solvent on binding affinity was probed by calculating binding energy changes in CH_3CN (ε=36.6) and DMSO (ε=47.2).~~ The results reveal that both selectors exhibited a higher affinity to AcO^- as

compared to chloride (Cl^-) and nitrate (NO_3^-) (Table 1). In addition, selector **2** showed stronger binding affinity toward AcO^- (ΔG = –5.24 kcal/mol in DMSO) than selector **1**(ΔG = –3.29 kcal/mol in DMSO), which is attributed to the improved hydrogen bonding for **2** as a result of the direct attachment of the electron withdrawing 3,5-bis(trifluoromethyl)phenyl group to the squaramide nitrogen. Slightly enhanced binding affinities for both selectors are observed in CH_3CN than in DMSO, which reflects an anticipated higher electrostatic attraction in a decreased dielectric constant.[37]

~~The computed geometries of the selectors-AcO^- are shown in Figure 2b. The hydrogen bonding between the AcO^- and N–H protons produces distances of N–H···O 1.64 Å and 1.66 Å for **1,** and 1.67 Å and 1.74 Å for **2**. As expected, slightly shorter bonding distances were observed for the N–H protons attached electron withdrawing aryls (highlighted in red in Figure 2b). Interestingly, the pyridinium moiety adopts a folded conformation to gain proximity to the anionic squaramide-AcO^- complex.~~

Binding constants were determined for model versions of selectors **1** and **2** (see Supporting Information) using the change in chemical shifts ($\Delta\delta$) of ^1H NMR titrations in DMSO-d_6. Initial addition of AcO^- induced a significant downfield shift (e.g., $\Delta\delta$ = 2.89 ppm for H_α) of **1**'s N–H protons (**Figure 2a**). Adding 1–3.2 equivalents of AcO^- resulted in sharper N–H proton signals, which is a result of strong hydrogen bonding interactions with AcO^-. The slightly downfield shift ($\Delta\delta$ = 0.1 ppm) of H_β for **1** may be the result of the folded structure as suggested by the DFT-calculated geometry. Similar hydrogen bonding interactions were observed with increasing Cl^- concentration (0.85–3.2 equiv) to produce a $\Delta\delta$ = 0.82 ppm (Figure S2). Both AcO^- and Cl^- form 1:1 binding stoichiometry with **1** according to Job plot analysis of the H_α chemical shifts (Figure S3). Minor chemical shifts induced by excess Br^- ($\Delta\delta$ = 0.14 ppm) and NO_3^- ($\Delta\delta$ = 0.05 ppm) and broad N–H proton signals indicate negligible interactions with the selector **1** (Figure S4 and S5). The binding constants are computed by fitting the chemical shifts of H_α based on 1:1 binding stoichiometry (Figure 2b

and Table 2). The high association constant observed for the selector **1** to AcO^- (K_a = 3.17×10^3 M^{-1}) and the relative binding trend $Cl^- > Br^- > NO_3^-$ is consistent with the DFT calculations.

Selector **2** displays significantly different binding characteristic toward AcO^- as revealed by ^1H NMR titration (Figure S6). After addition of 0.11 equivalents of AcO^-, the N–H proton signals disappear mainly as a result of deprotonation of N–H protons. In contrast, hydrogen bonding interactions are observed with added Cl^- and distinctive N–H proton signals exhibit a significant downfield chemical shift ($\Delta\delta$ = 1.21 ppm) (Figure S7). Selector **2** exhibits a 1:1 binding stoichiometry with Cl^- as confirmed by Job plot analysis (Figure S8). Similarly, a downfield chemical shift ($\Delta\delta$ = 0.29 ppm) with broadening of N–H proton signals was observed with Br^- addition (Figure S9). The broadening of N–H proton signals is attributed to the deprotonation of N–H protons,[38, 39] and the less acidic N–H on the pyridinium side of the squaramide is deprotonated after addition of 0.83 equiv Br^- (Figure S10). In contrast, the addition of NO_3^- resulted in the upfield chemical shift of N–H proton signals, which is attributed to reduced hydrogen bonding interactions caused by displacement of DMSO with NO_3^- (Figure S11). The binding constants for **2** toward Cl^- and Br^- were calculated from the NMR data (Figure 2c and Table 2) and revealed a stronger binding affinity for Cl^- over Br^-. Selector **2** has a 3.5-fold higher binding constant (K_a = 1.03×10^3 M^{-1}) for Cl^- when compared to **1**.

To further investigate binding characteristic of squaramide-based selectors with AcO^-, UV-vis titrations were performed in DMSO (Figure 2d-e). Upon the addition of 1 equiv of AcO^-, **1**'s major absorption band at 292 nm is slightly redshifted to 293 nm (Figure 2d). In addition, minor absorbance increase was observed at 372 nm. The absorbance profile with added AcO^- is consistent with a 1:1 binding stoichiometry (Figure S15) as determined by ^1H NMR titrations. The interacts of **1** are interpreted to be hydrogen bonding interactions between **1** and AcO^-.[40]

The absorption bands of **2** exhibited additional complexity upon sequential addition of AcO^- (Figure 2e). Decreased absorption bands at 280 nm, 325 nm, and 343 nm are observed with isosbestic points at 264 nm and 354 nm. In addition, a new absorption band was generated at 386 nm, which is assigned to an internal charge transfer transition.[41] The identical changes in **2**'s absorption spectra were observed upon the sequential addition of the strong base, tetrabutylammonium (TBA) hydroxide (Figure S16). This result is explained by an acid-base reaction inducing deprotonation of **2** by AcO^-.[42, 43] The deprotonation is visually confirmed by the color change to light yellow after addition of ~10 equiv of AcO^-, whereas very minor color changes are observed for **1** under similar conditions (Figure 2d-e inset). ~~The 1:1 binding stoichiometry is supported by the absorbance vs. mole fraction of AcO^- profile at 390 nm with the maximum hydrogen bonding interaction of 59% between **2** and AcO^-, i.e., **2**···AcO^-, after addition of 1 equiv of AcO^- (Figure S16a). This is in competition with deprotonation of **2** and, at a critical concentration, there is an abrupt decrease in the concentration of **2**···AcO^- as a result of the formation of $[H(AcO)_2]^-$, a hydrogen-bond self-complex (Figure S17b).~~[7] This result is consistent with the previous observations with squaramide-based receptors that experience deprotonation upon addition of basic anions F^- and AcO^-.[7] This effect is as expected more prevalent for receptors functionalized with electron withdrawing substituents such as nitrophenyl groups.[7]

In order to investigate the effect of pyridinium moiety on anion binding, a reference squaramide selector **3** was synthesized wherein the pyridinium is replaced by a hydroxyl group (Supporting Information). Selector **3** exhibits spectral changes similar to **2**'s upon addition of AcO^- and develops an absorption band at 386 nm and the two isosbestic points 264 nm and 356 nm (Figure S18). ~~Additionally, the binding stoichiometry of 1:1 complex was confirmed with a maximum hydrogen bonding interaction of 55% (**3**···AcO^-) at 1 equiv AcO^- and deprotonation occurs with the addition of more AcO^- to generate $[H(AcO)_2]^-$ (Figure S18b and c).~~ Quantitative comparison of equilibrium constants reveals that **2** exhibits ≈ 3-fold

higher AcO^- binding as compared to **3** (Table S2). ^1H NMR titration of **3** with Cl^- indicated a hydrogen bonding interaction with 1:1 binding stoichiometry confirmed by a Job plot (Figure S12-13). Similarly, approximately a 2.8-fold higher Cl^- association constant (K_a) was obtained for **2** relative to **3** (Figure S14 and Table S1). It is clear that pyridinium moiety contributes to stronger anion binding.

To further validate of our hypothesis of AcO^- acting as a base, the Brønsted acidity of the selectors were evaluated by direct pK_a measurement and computational modeling. Experimental pK_a values were determined by UV-vis titration with TBA benzoate in DMSO (Figure S19-21).[44] Theoretical pK_a values of the selectors were calculated by DFT using the SMD implicit solvation model,[45, 46] wherein the solution phase Gibbs free energies were calculated by combining free energies of solvation in DMSO with the gas phase free energies (Supporting Information). The experimental and computational pK_a values are within 1 pK_a unit and a consistent order of the selectors with **2** < **3** < **1** (Table 3). The squaramides with electron withdrawing 3,5-bis(trifluoromethyl)phenyl in **2** and **3** gives stronger acidity as compared to **1,** in which the 3,5-bis(trifluoromethyl)phenyl is separated by a methylene group. For this reason, **2** and **3** deprotonate upon addition of AcO^-, whereas **1** exhibits hydrogen bonding even with an excess (~5 equiv) of AcO^-. The comparison of **2** and **3** reveals that the electrostatic influence of the pyridinium lowers the pK_a value by ~1 pK_a unit.

Real-time anion sensors are prepared by squaramide functionalization of P4VP-SWCNT networks connecting proximate Au electrodes (Supporting Information and Figure S22). The alkylative functionalization of the P4VP pyridyl groups creates the proximate pyridinium moiety and covalently anchors **1** and **2** to the network. Specifically, squaramide having 3,5-bis(trifluoromethyl)benzyl group (P4VP-**1**-SWCNT) and 3,5-bis(trifluoromethyl)phenyl group (P4VP-**2**-SWCNT) were prepared on SWCNT networks covalently anchored to glass substrates. The functionalization of the selectors on the P4VP-SWCNT surface were confirmed by Fourier transform infrared (FTIR) spectroscopy and X-

ray photoelectron spectroscopy (XPS) (**Figure 3**). All samples including the model structures and the squaramide-functionalized P4VP-SWCNT exhibited a characteristic FTIR peak at 1793 cm^{-1}, which is the ring breathing mode of squaramide unit.[47] There is good agreement of the spectra from the model structures and selector functionalized P4VP-SWCNT, thereby confirming the structures (Figure 3a). High-resolution XPS N1*s* spectra of P4VP-**1**-SWCNT and P4VP-**2**-SWCNT display a characteristic pyridinium nitrogen peak at 402.2 eV (Figure 3b). The XPS N1*s* spectrum of the squaramide has peaks at 399.8 eV and 400.1 eV for P4VP-**1**-SWCNT and P4VP-**2**-SWCNT, respectively, and are in agreement with the model structures (Figure S23). It is noteworthy that a residual nitrogen peak (398.9 eV) from pyridine was not observed from N1*s* spectra confirming almost 100% conversion to pyridinium after functionalization with squaramide selectors (Figure S23).

Anion sensing characteristic was evaluated by injection of AcO^-, Cl^-, Br^-, and NO_3^- in acetonitrile (CH_3CN) at concentrations of 16.7–68.8 mM (**Figure 4**). Before injection of a solution, the initial resistances of the functionalized sensors were 85.23±8.43 kΩ and 42.42±8.94 kΩ for P4VP-**1**-SWCNT and P4VP-**2**-SWCNT, respectively, which was lower than the resistance (174.17±16.33 kΩ) of the pristine P4VP-SWCNT sensor (Figure S24). After injection of baseline solvent (i.e., CH_3CN), the resistance of the sensors was sharply increased more than 100% (Figure S25). Subsequently, real-time sensitivity transitions were observed upon injections of anion analytes with TBA salts dissolved in CH_3CN (Figure 4a and 4b). Stepwise increasing sensitivity was observed with increased analyte concentrations. Higher sensitivity transitions were obtained for P4VP-**1**-SWCNT to AcO^- at 16.7 mM with the sensitivity of 7.34% than $Cl^- > Br^- > NO_3^-$, which is consistent trend with the binding affinity from ^1H NMR (Figure 4a). In the case of P4VP-**2**-SWCNT, improved sensitivity was obtained toward AcO^- with 120.27% at 16.7 mM followed by the trend of $Br^- > Cl^- > NO_3^-$ (Figure 4b). The higher sensitivity of the P4VP-**2**-SWCNT to AcO^- is attributed to the internal charge transfer transition resulted from the deprotonation of selector. Although Cl^-

exhibited stronger binding than Br^- according to ^1H NMR titration, higher sensitivity transitions of P4VP-**2**-SWCNT to Br^- can be explained by the deprotonation of selector **2** with Br^- contrary to the formation of hydrogen bonding with Cl^-. The sensors exhibit reproduceable and improved AcO^- sensitivity using P4VP-**2**-SWCNT (Figure 4c) with the experimental limit of detection of 1.7 mM with the sensitivity of 31.82% (Figure S26).

Anion binding properties in the presence of water were investigated by ^1H NMR and UV-vis titrations (Figure S27). Similarly, deprotonation of the selector **2** was observed with AcO^- in DMSO-d_6 containing 10% water. However, 26% lower binding constant (K_a= 2.94 × 10^3 M^{-1}) was observed with decreased chemical shift (Δδ=0.11) in the presence of 10% water as compared to binding constant in 100% DMSO-d_6 (Figure S27a). UV-vis titration confirmed the selector **2** is less tend to be deprotonated in DMSO with 10% water (Figure S27b). Significant decrease in sensitivities of P4VP-**2**-SWCNT was observed toward AcO^- and Cl^- as increasing water contents (Figure S28). The decreasing sensitivities is mainly resulted from weakening ion-dipole interactions in water with high dielectric constant (ε=78) and the solvation of anions.[37] Anion sensing could not be performed in DMSO due to the solubility property of P4VP-**2**-SWCNT in DMSO resulting in reliability and reproducibility issues of the sensors.

Our anion sensing platform was demonstrated for real-time and portable anion sensing with a wireless sensing module that can transmit the sensing data to a smartphone. Two sensing electrodes connected by P4VP-**2**-SWCNT were connected to the wireless sensing module and resistance data was transmitted via near field communication (**Figure 5a** and Figure S29). Concentration dependency on AcO^- sensitivity was observed after injection of 2 μL of analyte with the concentrations ranging from 0.17–83.33 mM in CH_3CN. (Figure 5b). The limit of detectable concentration was 0.17 mM with the sensitivity of 12.39%. The anion sensing platform is connected with sensor arrays to detect multiple anions by simultaneous measurement of three resisters (R_1–R_3) (Figure 5c). Sequential injection of NO_3^-, Cl^-, and

AcO^- (2 μL each) in each sensor gives different sensitivity transitions, wherein AcO^- induces high sensitivity change while lower sensitive transitions were observed toward Cl^- and NO_3^-. The drift of the response signal was observed during the sensing of multiple anions, which was mainly attributed to the swelling of SWCNTs and P4VP in the organic solvent.[48, 49] Further optimization should be performed by controlling the coating thickness of P4VP-**2**-SWCNT to mitigate signal drift.

3. Conclusion

In summary, we have developed a real-time and wireless electrical transduction platform using noncovalently functionalized carbon nanotubes, which can efficiently transduce electrical signal generated from the chemical interaction between selectors and anion species. Asymmetric squaramide-based selectors having a cationic moiety (pyridinium) and an electron withdrawing 3,5-bis(trifluoromethyl)benzyl (**1**) and 3,5-bis(trifluoromethyl)phenyl (**2**) groups were synthesized and evaluated their anion binding properties. Binding studies based on ^{1}H NMR and UV-vis titrations revealed that the selector **1** exhibited hydrogen bonding interaction with binding order of $AcO^- > Cl^- > Br^- > NO_3^-$. In contrast, stronger binding affinity was obtained with selector **2** with $Br^- > Cl^- > NO_3^-$, whereas the selector was deprotonated with AcO^- (0.11 equiv). Comparative anion sensing studies were performed by functionalization of selectors **1** and **2** on the residual pyridyl groups of the surface anchored P4VP-SWCNT. The P4VP-SWCNT functionalized with selector **1** (P4VP-**1**-SWCNT) exhibited the sensitivity [$(R–R_0)/R_0$ (%)] of 7.34% at 16.7 mM AcO^-. On the other hand, an improved sensitivity of 120% at the same AcO^- concentration was obtained with P4VP-**2**-SWCNT. This result confirms that internal charge transfer by deprotonation as well as improving hydrogen bond donor properties by lowering pK_a of selectors are important factors to enhance sensitivity toward target anions. In addition, the cationic moiety formed after the functionalization of selectors is beneficial in anion binding

through direct interaction with anions as well as lowering acidity. Finally, wireless detection of anions was demonstrated using the P4VP-**2**-SWCNT sensor by integration with near field communication sensing module and transmitting the data to a smartphone. High sensitivity transitions with the limit of detection of 0.17 mM AcO^- as well as sensor arrays for sensing of various anions were achieved with 2 μL of the analyte solution. This work paves a new way for portable and real-time anion sensing by combination of electrostatic and hydrogen bonding interactions to efficiently transduce anion complexation into electrical signal.

4. Experimental Section

***Materials*:** All chemicals, reagents and SWCNTs (CoMoCAT SWCNTs with an average diameter of 0.82 nm, ≥89% carbon basis, ≥99% as carbon nanotubes, lot #: MKBP333V) were purchased from Sigma-Aldrich and used without additional purification. 3,5-bis(trifluoromethyl)benzylamine, 3,5-bis(trifluoromethyl)aniline, 3-bromopropylamine hydrobromide, 3-amino-1-propanol, 3,4-dimethoxycyclobut-3-ene-1,2-dione, and pyridine were purchased from Sigma-Aldrich. Deuterated solvents for NMR spectroscopy was purchased from Cambridge Isotope Laboratories, Inc. 3-bromopropyltrichlorosilane was purchased from Gelest. 3,4-diethoxycyclobut-3-ene-1,2-dione was purchased from TCI Chemical.

Synthesis of 3-((3,5-bis(trifluoromethyl)phenyl)amino)-4-methoxycyclobut-3-ene-1,2-dione: A stirred solution of 3,4-dimethoxycyclobut-3-ene-1,2-dione (500 mg, 3,5205 mmol) and zinc trifluoromethanesulfonate (256 mg, 0.7041 mmol, 20 mol %) in toluene/DMF 19:1 (20 mL) was added 3,5-bis(trifluoromethyl)aniline (522 µL, 3.444 mmol). The solution was heated to 100 °C and stirred for 15 h. After cooling, the mixture was filtered and concentrated the filtrate in vacuum. The product was obtained after washing with water and filtered. Yield: 921 mg (2.7165 mmol, 77%). ^{1}H NMR (400 MHz, DMSO-d_6) δ 11.18 (s, 1H), 10.62 (s, 1H), 8.04 (s, 2H), 7.88 (s, 2H), 7.79 (s, 1H), 7.70 (s, 1H), 4.41 (s, 3H). HRMS (DART+, *m/z*) calculated for $C_{13}H_8F_6NO_3$ $[M+H]^+$=340.0408 Observed 340.0403.

Synthesis of 3-((3,5-bis(trifluoromethyl)phenyl)amino)-4-((3-bromopropyl)amino)cyclobut-3-ene-1,2-dione: *3-((3,5-bis(trifluoromethyl)phenyl)amino)-4-methoxycyclobut-3-ene-1,2-dione* (200 mg, 0.5899 mmol) was dissolved in 10 mL MeOH and the solution was added 3-bromopropylamine hydrobromide (200 mg, 0.7079 mmol) followed by triethylamine (99 µL, 0.7079 mmol). After the stirring for 3d at 70 °C, the solution was concentrated and redispersed in water. The mixture was filtered and dried. Yield: 218 mg (0.4910 mmol, 87%). ^{1}H NMR (400 MHz, DMSO-d_6) δ 10.18 (s, 1H), 8.01 (s, 2H), 7.76 (s, 1H), 7.67 (s, 1H), 3.73 (d, J = 6.3 Hz, 2H), 3.60 (t, J = 6.6 Hz, 2H), 2.13 (p, J = 6.6 Hz, 2H). HRMS (DART+, *m/z*) calculated for $C_{15}H_{12}BrF_6N_2O_2$ $[M+H]^+$=444.9986 Observed 444.9973.

Synthesis of 1-(3-((2-((3,5-bis(trifluoromethyl)phenyl)amino)-3,4-dioxocyclobut-1-en-1-yl)amino)propyl)pyridin-1-ium: *3-((3,5-bis(trifluoromethyl)phenyl)amino)-4-((3-bromopropyl)amino)cyclobut-3-ene-1,2-dione* (50 mg, 0.1126 mmol) was dissolved in 5 mL anhydrous acetonitrile and the solution was added pyridine (27 µL, 0.3378 mmol). The

mixture was refluxed for 20 h and concentrated in vacuum. The product was redispersed in ethyl acetate and filtered. Yield: 28 mg (0.0535 mmol, 48%). ^{1}H NMR (400 MHz, DMSO-d_6) δ 10.40 (s, 1H), 9.10 (d, J = 6.0 Hz, 2H), 8.62 (t, J = 7.8 Hz, 1H), 8.19 (d, J = 6.9 Hz, 2H), 8.04 (s, 3H), 7.85 (s, 1H), 7.69 (s, 1H), 4.71 (t, J = 7.3 Hz, 2H), 3.74 – 3.62 (m, 3H), 2.28 (p, J = 13.9, 6.9 Hz, 2H). ^{13}C NMR (126 MHz, DMSO-d_6) δ 184.32, 180.17, 169.86, 162.88, 148.87, 145.63, 144.91, 141.26, 131.38 (q, J = 33.2, 32.6 Hz), 128.19, 123.15 (q, J = 273.0 Hz), 117.62, 114.71 (t, J = 3.6 Hz), 58.14, 40.59, 31.81. HRMS (DART+, *m/z*) calculated for $C_{20}H_{16}F_6N_3O_2$ $[M]^+$=444.1147 Observed 444.1136.

Functionalization of squaramide-based selectors: The surface reaction was performed to functionalize the squaramide-based selectors. A solution of **2** (10 mg) in acetonitrile (12 mL) was prepared to obtain P4VP-SWCNT functionalized with selector **1** (P4VP-**1**-SWCNT). The glass substrate with the surface anchored P4VP-SWCNT was immersed in the solution. Then, the solution was heated to 85 °C for 24 h to ensure quaternization reactions with residual pyridyl groups from P4VP and bromide groups from **2**. For the functionalization of selector **2** (P4VP-**2**-SWCNT), the identically process was carried out by dissolving **5** in acetonitrile.

Anion sensing measurement: Anion sensing characteristic of P4VP-SWCNT functionalized by squaramide-based selectors were evaluated toward AcO^-, Cl^-, Br^-, and NO_3^- in acetonitrile. As a baseline solvent, acetonitrile (10 μL) was injected in a chamber to obtain constant baseline resistance. Once the baseline resistance is stabilized, analyte solution (0.1 M) was introduced to the camber by sequentially increasing concentrations, i.e., 2 μL, 4 μL, 6 μL, and 10 μL. Resistance transitions were recorded in real-time during the injection of analyte. The sensitivity was evaluated by the normalized resistance changes, i.e., $S=(R–R_0)/R_0$ (%), where R is the resistance under injection of an analyte and R_0 is the baseline resistance of anion sensors before injection of an analyte.

Supporting Information
Supporting Information is available from the Wiley Online Library or from the author.

Acknowledgements

This material is based on work supported by the U.S. Army Engineer Research and Development Center Environmental Quality Technology Program under contract W912HZ-17-2-0027 and conducted at Massachusetts Institute of Technology. B.Y. was supported by an appointment to the Postgraduate Research Participation Program at CCDC–SC administered by the Oak Ridge Institute for Science and Education through an interagency agreement between the U.S. Department of Energy and CCDC–SC.

Received: ((will be filled in by the editorial staff))
Revised: ((will be filled in by the editorial staff))
Published online: ((will be filled in by the editorial staff))

References

[1] N. H. Evans, P. D. Beer, *Angew. Chem. Int. Ed.* **2014**, 53, 11716.

[2] N. Busschaert, C. Caltagirone, W. Van Rossom, P. A. Gale, *Chem. Rev.* **2015**, 115, 8038.

[3] P. A. Gale, E. N. W. Howe, X. Wu, M. J. Spooner, *Coordin. Chem. Rev.* **2018**, 375, 333.

[4] A. J. Wolfe, *Microbiol. Mol. Biol. R* **2005**, 69, 12.

[5] M. De Mey, S. De Maeseneire, W. Soetaert, E. Vandamme, *J. Ind. Microbiol. Biot.* **2007**, 34, 689.

[6] D. H. Choi, Y. Li, G. R. Cutting, P. C. Searson, *Sens. Actuators B* **2017**, 250, 673.

[7] V. Amendola, G. Bergamaschi, M. Boiocchi, L. Fabbrizzi, M. Milani, *Chem. Eur. J.* **2010**, 16, 4368.

[8] D. Quinonero, R. Prohens, C. Garau, A. Frontera, P. Ballester, A. Costa, P. M. Deya, *Chem. Phys. Lett.* **2002**, 351, 115.

[9] X. Ni, X. Li, Z. Wang, J. P. Cheng, *Org. Lett.* **2014**, 16, 1786.

[10] J. M. Ho, V. E. Zwicker, K. K. Y. Yuen, K. A. Jolliffe, *J. Org. Chem.* **2017**, 82, 10732.

[11] A. Rostami, A. Colin, X. Y. Li, M. G. Chudzinski, A. J. Lough, M. S. Taylor, *J. Org. Chem.* **2010**, 75, 3983.

[12] N. Busschaert, I. L. Kirby, S. Young, S. J. Coles, P. N. Horton, M. E. Light, P. A. Gale, *Angew. Chem. Int. Ed.* **2012**, 51, 4426.

[13]X. P. Bao, X. Wu, S. N. Berry, E. N. W. Howe, Y. T. Chang, P. A. Gale, *Chem. Commun.* **2018**, 54, 1363.

[14] V. Fernandez-Moreira, J. V. Alegre-Requena, R. P. Herrera, I. Marzo, M. C. Gimeno, *RSC Adv.* **2016**, 6, 14171.

[15] J. Aleman, A. Parra, H. Jiang, K. A. Jorgensen, *Chem. Eur. J.* **2011**, 17, 6890.

[16] S. M. Banik, A. Levina, A. M. Hyde, E. N. Jacobsen, *Science* **2017**, 358, 761.

[17] P. Blondeau, M. Segura, R. Perez-Fernandez, J. de Mendoza, *Chem. Soc. Rev.* **2007**, 36, 198.

[18] Z. Xu, S. K. Kim, J. Yoon, *Chem. Soc. Rev.* **2010**, 39, 1457.

[19] J. Yoon, S. K. Kim, N. J. Singh, K. S. Kim, *Chem. Soc. Rev.* **2006**, 35, 355.

[20] E. Mulugeta, Q. He, D. Sareen, S. J. Hong, J. H. Oh, V. M. Lynch, J. L. Sessler, S. K. Kim, C. H. Lee, *Chem.* **2017**, 3, 1008.

[21] G. Bergamaschi, M. Boiocchi, E. Monzani, V. Amendola, *Org. Biomol. Chem.* **2011**, 9, 8276.

[22] N. L. Kilah, P. D. Beer, Anion Recognition in Supramolecular Chemistry; **2010**; Chapter 33, pp 301-340.

[23] K. S. Jeong, Y. L. Cho, *Tetrahedron Lett* **1997**, 38, 3279.

[24] K. Hirose, Determination of Binding Constants In *Analytical Methods in Supramolecular Chemistry*; **2007**; Chapter 2, pp 17-54

[25] L. H. Perruchoud, A. Hadzovic, X. A. Zhang, *Chem. Eur. J.* **2015**, 21, 8711.

[26] B. R. Mullaney, M. J. Cunningham, J. J. Davis, P. D. Beer, *Polyhedron* **2016**, 116, 20.

[27] R. Hein, A. Borissov, M. D. Smith, P. D. Beer, J. J. Davis, *Chem. Commun.* **2019**, 55, 4849.

[28] J. Y. C. Lim, M. J. Cunningham, J. J. Davis, P. D. Beer, *Chem. Commun.* **2015**, 51, 14640.

[29] V. Schroeder, S. Savagatrup, M. He, S. B. Ling, T. M. Swager, *Chem. Rev.* **2019**, 119, 599.

[30] J. F. Fennell, S. F. Liu, J. M. Azzarelli, J. G. Weis, S. Rochat, K. A. Mirica, J. B. Ravnsbaek, T. M. Swager, *Angew. Chem. Int. Ed.* **2016**, 55, 1266.

[31] C. H. Park, V. Schroeder, B. J. Kim, T. M. Swager, *ACS Sens.* **2018**, 3, 2432.

[32] S. Savagatrup, V. Schroeder, X. He, S. B. Lin, M. He, O. Yassine, K. N. Salama, X. X. Zhang, T. M. Swager, *Angew. Chem. Int. Ed.* **2017**, 56, 14066.

[33] B. Yoon, S. F. Liu, T. M. Swager, *Chem. Mater.* **2016**, 28, 5916.

[34] R. Zhu, M. Desroches, B. Yoon, T. M. Swager, *ACS Sens.* **2017**, 2, 1044.

[35] B. Yoon, S. J. Choi, T. M. Swager, G. F. Walsh, *ACS Appl. Mater. Interfaces* **2018**, 10, 33373.

[36] S. Soylemez, B. Yoon, L. Toppare, T. M. Swager, *ACS Sens.* **2017**, 2, 1123.

[37] S. Kubik, *Chem. Soc. Rev.* **2010**, 39, 3648.

[38] K. N. Farrugia, D. Makuc, A. Podborska, K. Szacilowski, J. Plavec, D. C. Magri, *Org. Biomol. Chem.* **2015**, 13, 1662.

[39] S. K. Dey, M. Al Kobaisi, S. V. Bhosale, *Chemistryopen* **2018**, 7, 934.

[40] V. Amendola, L. Fabbrizzi, L. Mosca, *Chem. Soc. Rev.* **2010**, 39, 3889.

[41] M. Boiocchi, L. Del Boca, D. E. Gomez, L. Fabbrizzi, M. Licchelli, E. Monzani, *J. Am. Chem. Soc.* **2004**, 126, 16507.

[42] C. Jin, M. Zhang, C. Deng, Y. F. Guan, J. Gong, D. R. Zhu, Y. Pan, J. L. Jiang, L. Y. Wang, *Tetrahedron Lett.* **2013**, 54, 796.

[43] C. Perez-Casas, A. K. Yatsimirsky, *J. Org. Chem.* **2008**, 73, 2275.

[44]A. Jeppesen, B. E. Nielsen, D. Larsen, O. M. Akselsen, T. I. Solling, T. Brock-Nannestad, M. Pittelkow, *Org. Biomol. Chem.* **2017**, 15, 2784.

[45] B. Thapa, H. B. Schlegel, *J. Phys. Chem. A* **2016**, 120, 5726.

[46] V. E. Zwicker, K. K. Y. Yuen, D. G. Smith, J. M. Ho, L. Qin, P. Turner, K. A. Jolliffe, *Chem. Eur. J.* **2018**, 24, 1140.

[47] C. Q. Tong, T. X. Liu, V. S. Talens, W. E. M. Noteborn, T. H. Sharp, M. M. R. M. Hendrix, I. K. Voets, C. L. Mummery, V. V. Orlova, R. E. Kieltyka, *Biomacromolecules* **2018**, 19, 1091.

[48] S. B. Lin, T. M. Swager, *ACS Sens.* **2018**, 3, 569.

[49] D. Hines, M. H. Rummeli, D. Adebimpe, D. L. Akins, *Chem. Commun.* **2014**, 50, 11568.

Figure Captions

Figure 1. Schematic illustrations of (a) chemiresistive-type anion sensing platform and (b) chemical structure of immobilized P4VP-SWCNT on a glass substrate with the functionalization of anion binding selectors

Figure 2. (a) Transitions of ^{1}H NMR spectra of selector **1** upon sequential addition of AcO^- (0–3.2 equiv) in DMSO-d_6. Chemical shifts of a N–H proton upon addition of anions such as AcO^-, Cl^-, Br^-, and NO_3^- in DMSO-d_6: (a) selector **1** and (b) selector **2**. UV-vis titration of (d) selector **1** ([**1**]= 4.4×10^{-5} M) and (e) selector **2** ([**2**]= 4.5×10^{-5} M) by the subsequent addition of AcO^- (0–1 equiv) in DMSO. Anions were added as tetrabutylammonium (TBA) salts.

Figure 3. (a) ATR-FTIR spectra of the pristine P4VP-SWCNT, P4VP-**1**-SWCNT, and P4VP-**2**-SWCNT on glass substrates as well as model structures of selector **1** and **2**. X-ray photoelectron spectroscopy (XPS) spectra of (b) P4VP-**1**-SWCNT and (c) P4VP-**2**-SWCNT on glass substrates.

Figure 4. Dynamic sensitivity transitions of (a) P4VP-**1**-SWCNT and (b) P4VP-**2**-SWCNT toward anions in the concentration range of 16.7–68.8 mM in (CH_3CN). (c) Summary of sensitivity properties with pristine P4VP-SWCNT and the squaramide-based selector functionalized P4VP-SWCNT at different anion concentrations.

Figure 5. (a) Real-time and wireless detection of anions by integration of anion sensing platform and wireless data transmitting module. (b) Wireless anion sensing property of P4VP-**2**-SWCNT toward AcO^- in the concentration range of 0.17–83.33 mM in CH_3CN. (c) Continuous anion sensing with sensor arrays patterned with P4VP-**2**-SWCNT. (One data sampling ~1 sec)

<Figure 1>

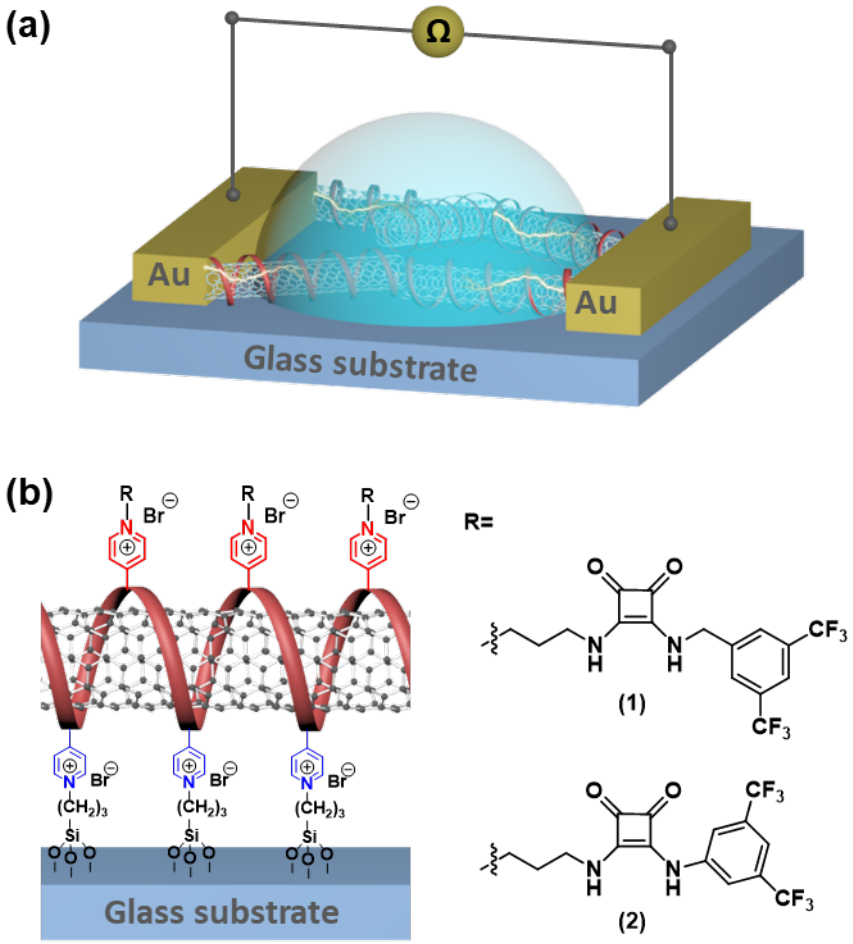
(a)
Ω
Au
Au
Glass substrate
(b)
R
Br
Si
(CH2)3
Glass substrate
R=
(1)
(2)
CF3

<Figure 2>

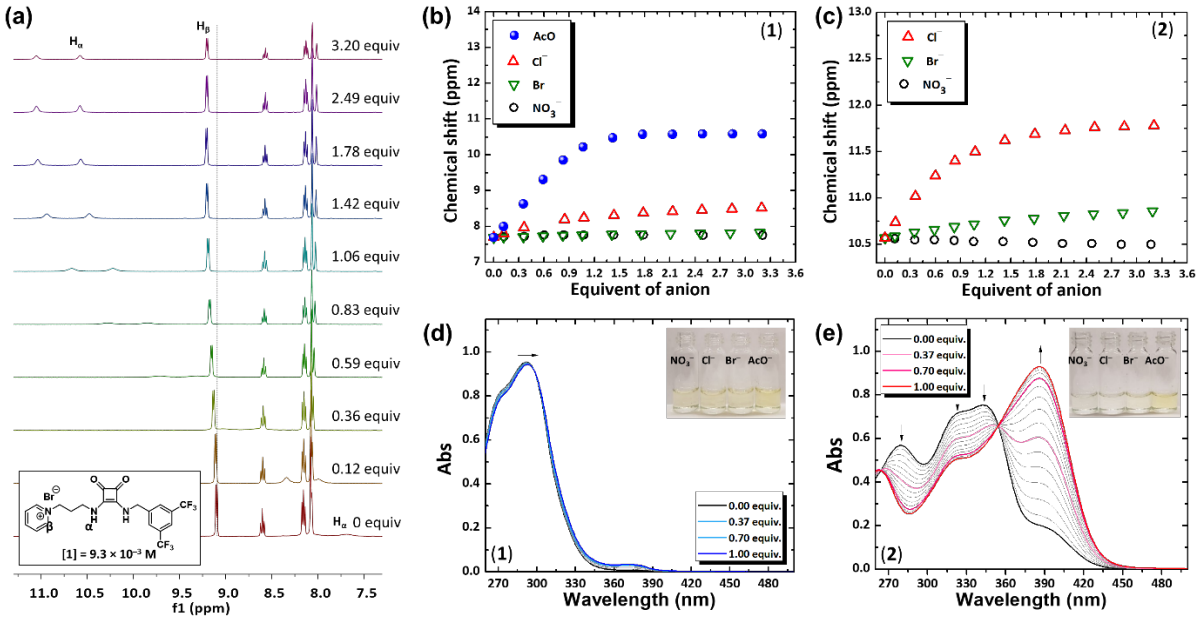
(a)
Hα
Hβ
3.20 equiv
2.49 equiv
1.78 equiv
1.42 equiv
1.06 equiv
0.83 equiv
0.59 equiv
0.36 equiv
0.12 equiv
Hα 0 equiv
[1] = 9.3 × 10⁻³ M
11.0 10.5 10.0 9.5 9.0 8.5 8.0 7.5
f1 (ppm)
(b)
AcO⁻
Cl⁻
Br⁻
NO3⁻
(1)
Chemical shift (ppm)
Equivent of anion
(c)
Cl⁻
Br⁻
NO3⁻
(2)
Chemical shift (ppm)
Equivent of anion
(d)
NO3⁻ Cl⁻ Br⁻ AcO⁻
0.00 equiv.
0.37 equiv.
0.70 equiv.
1.00 equiv.
(1)
Abs
Wavelength (nm)
(e)
0.00 equiv.
0.37 equiv.
0.70 equiv.
1.00 equiv.
NO3⁻ Cl⁻ Br⁻ AcO⁻
(2)
Abs
Wavelength (nm)

<Figure 3>

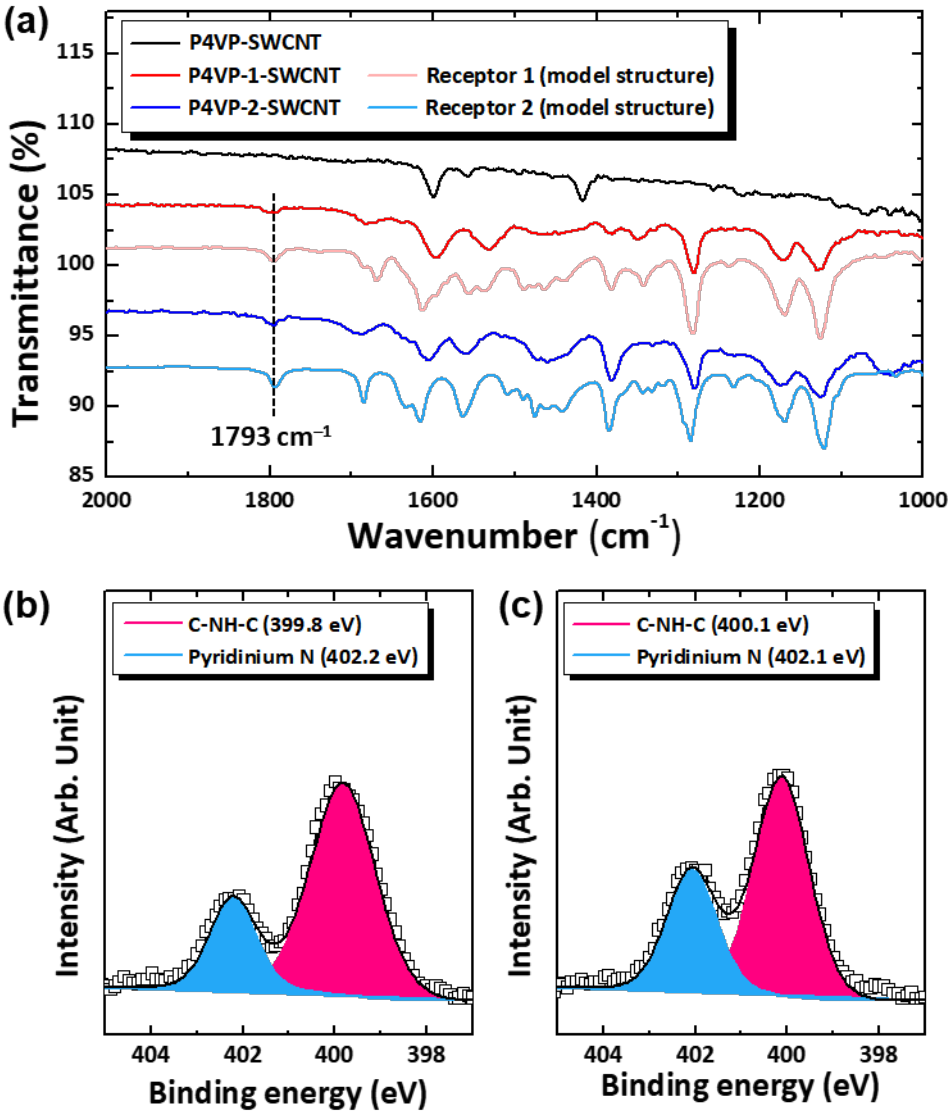
(a)
P4VP-SWCNT
P4VP-1-SWCNT
P4VP-2-SWCNT
Receptor 1 (model structure)
Receptor 2 (model structure)
Transmittance (%)
1793 cm⁻¹
Wavenumber (cm⁻¹)
(b)
C-NH-C (399.8 eV)
Pyridinium N (402.2 eV)
Intensity (Arb. Unit)
Binding energy (eV)
(c)
C-NH-C (400.1 eV)
Pyridinium N (402.1 eV)
Intensity (Arb. Unit)
Binding energy (eV)

<Figure 4>

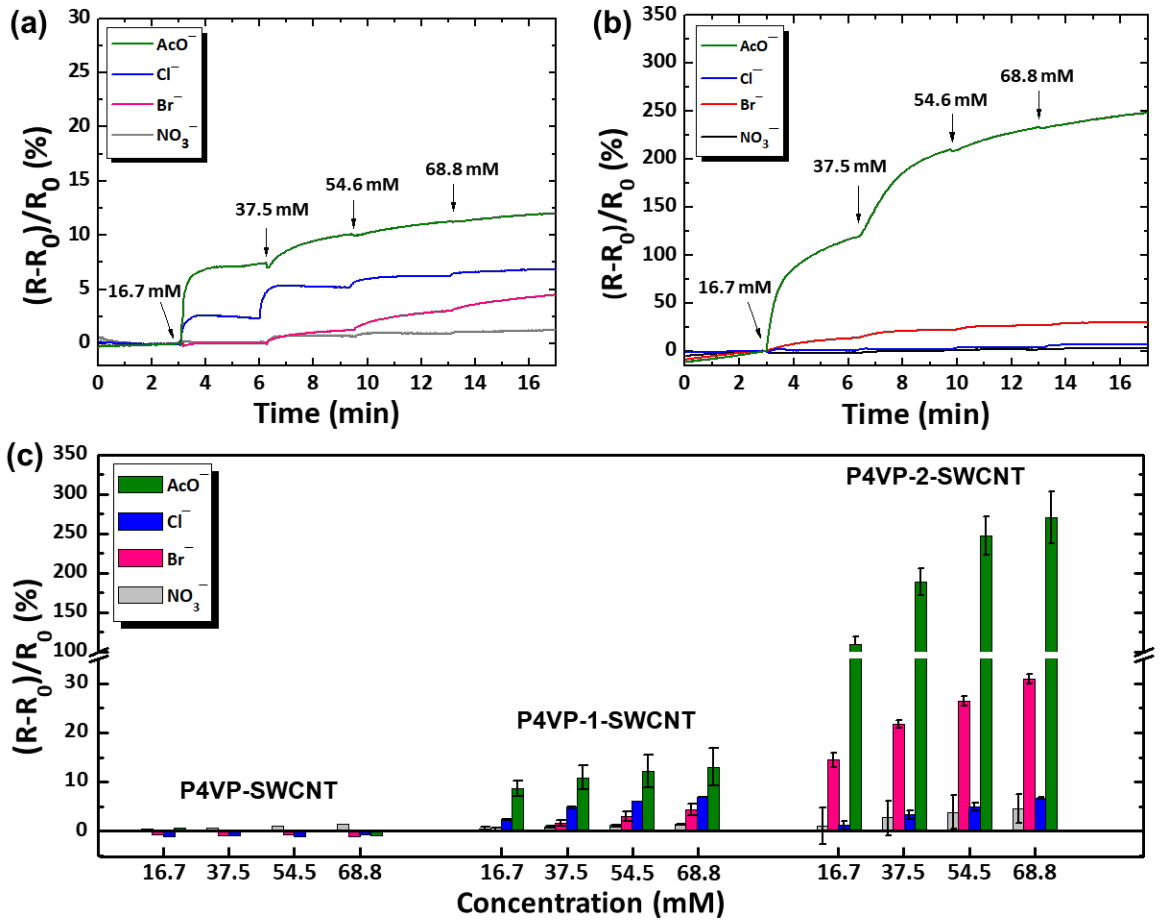
(a)
AcO⁻
Cl⁻
Br⁻
NO3⁻
16.7 mM
37.5 mM
54.6 mM
68.8 mM
(R-R0)/R0 (%)
Time (min)
(b)
AcO⁻
Cl⁻
Br⁻
NO3⁻
16.7 mM
37.5 mM
54.6 mM
68.8 mM
(R-R0)/R0 (%)
Time (min)
(c)
AcO⁻
Cl⁻
Br⁻
NO3⁻
P4VP-SWCNT
P4VP-1-SWCNT
P4VP-2-SWCNT
(R-R0)/R0 (%)
16.7 37.5 54.5 68.8
Concentration (mM)

<Figure 5>

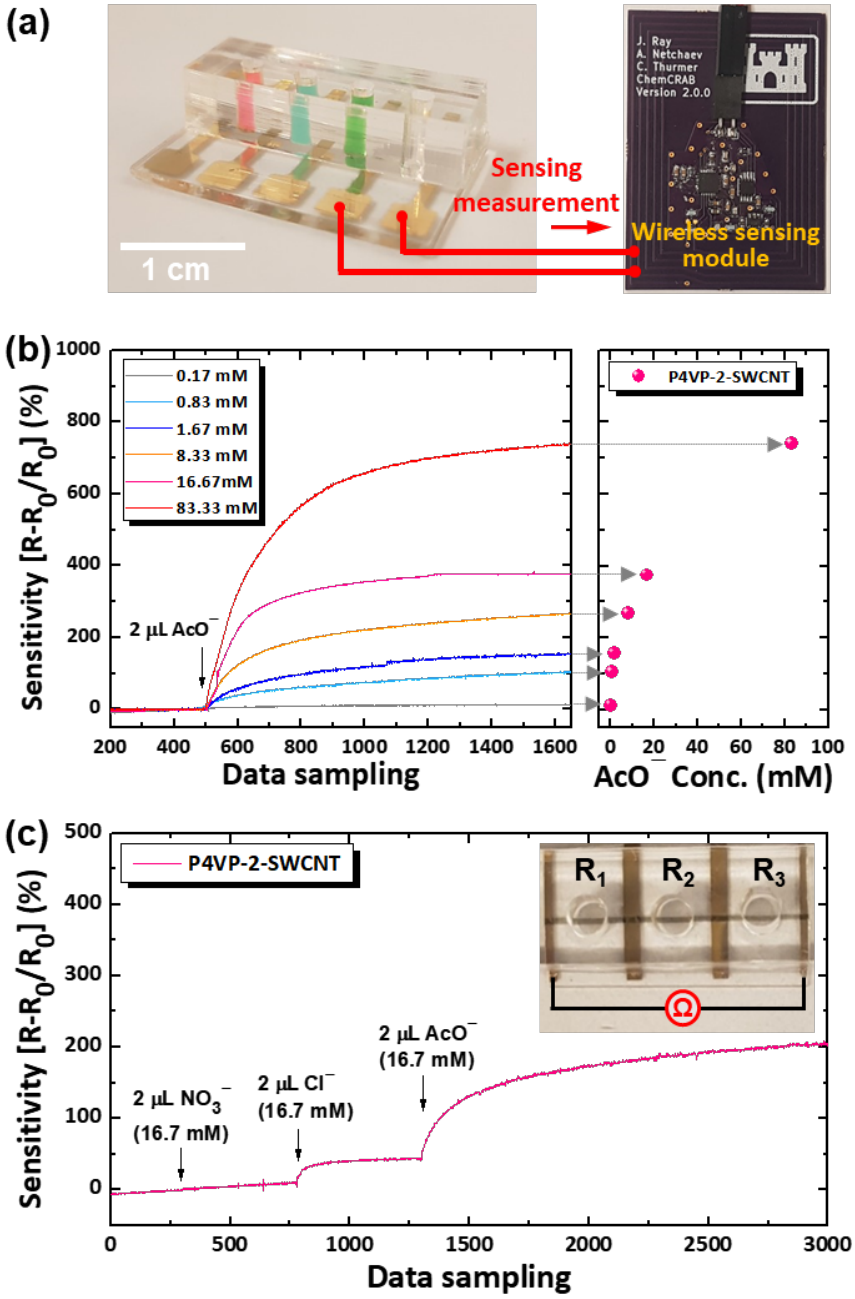
(a)
1 cm
Sensing measurement
Wireless sensing module
J. Ray
A. Netchaev
C. Thurmer
ChemCRAB
Version 2.0.0
(b)
Sensitivity [R-R0/R0] (%)
0.17 mM
0.83 mM
1.67 mM
8.33 mM
16.67mM
83.33 mM
2 μL AcO⁻
Data sampling
P4VP-2-SWCNT
AcO⁻ Conc. (mM)
(c)
Sensitivity [R-R0/R0] (%)
P4VP-2-SWCNT
R1
R2
R3
2 μL NO3⁻ (16.7 mM)
2 μL Cl⁻ (16.7 mM)
2 μL AcO⁻ (16.7 mM)
Data sampling

Table 1. DFT-calculated free energy changes (ΔG) of selectors after binding with anions in CH_3CN and DMSO.

Anion X^-	ΔG [kcal/mol]			
	Selector 1		Selector 2	
	DMSO	CH_3CN	DMSO	CH_3CN
AcO^-	-3.29	-3.34	-5.24	-5.29
Cl^-	-0.70	-0.74	-1.29	-1.32
NO_3^-	1.60	1.61	0.33	0.33

Table 2. Association constant (K_a) of squaramide-based selectors determined by ^{1}H NMR titration in DMSO-d_6 at 298 K.

	Anion X^-	**AcO^-**	**Cl^-**	**Br^-**	**NO_3^-**
Selector 1	K_a [M^{-1}]	3.20×10^3	2.99×10^2	57.64	5.20×10^{-5}
	Δδ (**1**)	2.89	0.85	0.14	0.06
Selector 2	K_a [M^{-1}]	-[d]	1.03×10^3	67.71[d]	58.56
	Δδ (**2**)	-	1.21	0.29	-0.07

Anions were added as TBA salts. Chemical shift (Δδ) data was calculated based on the shift of a N–H proton after addition of ~3.2 eq anion. '*d*' is deprotonation of selector after addition of certain equiv of anion. Estimated error in K_a <15%.

Table 3. Experimental and calculated pK_a values for the squaramide-based selectors

	pK_a	
	Experiment	**Calculation**
Selector **1**	13.89 ± 0.03	13.48
Selector **2**	10.02 ± 0.21	9.89
Selector **3**	10.97 ± 0.04	10.06

Experimental pK_a values were determined by UV-vis titration upon addition of TBA benzoate in DMSO. Error is based on propagation of error on equilibrium constant (K_{eq}). Calculated pK_a values were determined in DMSO.

The table of contents entry

Electrical transduction platform using single-walled carbon nanotubes (SWCNTs) noncovalently functionalized with squaramide-based anion binding selectors was developed for real-time wireless anion detection. Improved anion sensitivity was achieved by internal charge transfer after deprotonation of squaramide selector upon addition of acetate.

Keyword

Single-walled carbon nanotubes; squaramide; anion sensing; hydrogen bonding; deprotonation

*By Seon-Jin Choi, Bora Yoon, Jason D. Ray, Anton Netchaev, Lee C. Moores, and Timothy M. Swager**

Title

Chemiresistors for the Real-Time Wireless Detection of Anions

ToC figure